JPn Neuroscience

The Journal of Physiology

J Physiol 591.10 (2013) pp 2687–2703

Physiological and morphological properties of *Dbx1*-derived respiratory neurons in the pre-Bötzinger complex of neonatal mice

Maria Cristina D. Picardo, Krishanthi T. H. Weragalaarachchi, Victoria T. Akins and Christopher A. Del Negro

Department of Applied Science, The College of William & Mary, Williamsburg, VA, USA

Key points

- The transcription factor *Dbx1* gives rise to putatively respiratory rhythm-generating neurons in the pre-Bötzinger complex. Comparative analysis of *Dbx1*-derived (*Dbx1*$^+$) and non-*Dbx1*-derived (*Dbx1*$^-$) neurons can help elucidate the cellular bases of respiratory rhythm generation.
- *In vitro*, *Dbx1*$^+$ neurons activate earlier in the respiratory cycle, discharge larger magnitude inspiratory bursts and exhibit a lower rheobase compared with *Dbx1*$^-$ neurons.
- The *Dbx1*$^+$ neurons tend to express the intrinsic currents I_A (transient outward A-current) and I_h (hyperpolarization-activated current) in diametric opposition, which may facilitate temporal summation of excitatory synaptic inputs, whereas the *Dbx1*$^-$ neurons show no significant pattern of expression regarding I_A and I_h.
- The *Dbx1*$^+$ neurons exhibit smooth, spineless dendrites that project in the transverse plane, whereas the *Dbx1*$^-$ neurons are confined to the transverse plane to a lesser extent and sometimes exhibit spines.
- The properties of *Dbx1*$^+$ neurons that may contribute to respiratory rhythmogenesis include a high level of excitability linked to ongoing network activity and dendritic properties that may facilitate synaptic integration.

Abstract Breathing in mammals depends on an inspiratory-related rhythm that is generated by glutamatergic neurons in the pre-Bötzinger complex (preBötC) of the lower brainstem. A substantial subset of putative rhythm-generating preBötC neurons derive from a single genetic line that expresses the transcription factor *Dbx1*, but the cellular mechanisms of rhythmogenesis remain incompletely understood. To elucidate these mechanisms, we carried out a comparative analysis of *Dbx1*-expressing neurons (*Dbx1*$^+$) and non-*Dbx1*-derived (*Dbx1*$^-$) neurons in the preBötC. Whole-cell recordings in rhythmically active newborn mouse slice preparations showed that *Dbx1*$^+$ neurons activate earlier in the respiratory cycle and discharge greater magnitude inspiratory bursts compared with *Dbx1*$^-$ neurons. Furthermore, *Dbx1*$^+$ neurons required less input current to discharge spikes (rheobase) in the context of network activity. The expression of intrinsic membrane properties indicative of A-current (I_A) and hyperpolarization-activated current (I_h) tended to be mutually exclusive in *Dbx1*$^+$ neurons. In contrast, there was no such relationship in the expression of currents I_A and I_h in *Dbx1*$^-$ neurons. Confocal imaging and digital morphological reconstruction of recorded neurons revealed dendritic spines on *Dbx1*$^-$ neurons, but *Dbx1*$^+$ neurons were spineless. The morphology of *Dbx1*$^+$ neurons was largely confined to the transverse plane, whereas *Dbx1*$^-$ neurons projected dendrites to a greater extent in the parasagittal plane. The putative rhythmogenic nature of *Dbx1*$^+$ neurons may be attributable,

DOI: 10.1113/jphysiol.2012.250118

in part, to a higher level of intrinsic excitability in the context of network synaptic activity. Furthermore, *Dbx1*$^+$ neuronal morphology may facilitate temporal summation and integration of local synaptic inputs from other *Dbx1*$^+$ neurons, taking place largely in the dendrites, which could be important for initiating and maintaining bursts and synchronizing activity during the inspiratory phase.

(Received 14 December 2012; accepted after revision 27 February 2013; first published online 4 March 2013)
Corresponding author C. A. Del Negro: Department of Applied Science, McGlothlin-Street Hall, Room 318, The College of William & Mary, Williamsburg, VA 23187-8795, USA. Email: cadeln@wm.edu

Abbreviations ACSF, artificial cerebrospinal fluid; C_M, whole-cell capacitance; E, embryonic day; FFA, flufenamic acid; I_A, transient outward A-current; I_{CAN}, calcium-activated non-specific cation current; I_h, hyperpolarization-activated current; I_{NaP}, persistent sodium current; IR-DIC, infrared-enhanced differential interference contrast; P, postnatal day; preBötC, pre-Bötzinger complex; R_N, input resistance; τ_M, membrane time constant; *V*–*I*, voltage–current; XII, hypoglossal (12th) cranial nerve.

Introduction

The pre-Bötzinger complex (preBötC) of the ventrolateral medulla contains the neurons that generate the inspiratory phase of the respiratory rhythm (Smith *et al.* 1991; Feldman & Del Negro, 2006). Rhythm generation depends on glutamatergic neurons, as well as neurons that express neuropeptides and peptide receptors (Gray *et al.* 1999, 2001; Wallen-Mackenzie *et al.* 2006; Tan *et al.* 2008). Neurons with glutamatergic and peptidergic transmitter phenotypes that also express peptide receptors form a superset of neurons from the same genetic lineage. In the mouse embryo, the homeobox gene *Dbx1* controls the fate of glutamatergic commissural interneurons in the hindbrain, including rhythm-generating preBötC neurons (Bouvier *et al.* 2010; Gray *et al.* 2010). In the absence of *Dbx1*, the preBötC does not form, and mouse pups die at birth without taking a breath or making any respiratory movements whatsoever (Pierani *et al.* 2001; Bouvier *et al.* 2010; Gray *et al.* 2010). We hypothesize that the intrinsic and morphological features that differentiate *Dbx1*-derived (*Dbx1*$^+$) neurons from non-*Dbx1*-derived (*Dbx1*$^-$) neurons, which are probably GABAergic or glycinergic preBötC neurons (Kuwana *et al.* 2006; Winter *et al.* 2009; Morgado-Valle *et al.* 2010), may help to elucidate the cellular mechanisms of respiratory rhythmogenesis in the preBötC.

Brainstem slices containing the preBötC spontaneously generate inspiratory motor patterns *in vitro* that can be monitored via the hypoglossal (XII) cranial nerve (Smith *et al.* 1991; Feldman & Del Negro, 2006; Feldman *et al.* 2013). Previous studies have investigated the membrane properties implicated in rhythm generation, although without regard to the genotype or transmitter phenotype of the preBötC neurons studied. During a respiratory cycle *in vitro* that generally lasts 5–10 s, putatively rhythmogenic neurons are the earliest to activate, depolarizing and starting to discharge spikes approximately 400 ms prior to the inspiratory phase marked by XII motor output (Rekling *et al.* 1996*a*; Thoby-Brisson & Ramirez, 2001). The presence of a transient outward current, i.e. A-current (I_A), and the lack of a hyperpolarization-activated mixed cationic current, i.e. h-current (I_h), have also been hypothesized to influence inspiratory burst generation by promoting orderly recruitment of constituent rhythmogenic neurons and preventing spurious discharge (Rekling *et al.* 1996*a*; Hayes *et al.* 2008). Neurons distributed throughout the ventral respiratory brainstem networks, including the preBötC, express persistent Na^+ current (I_{NaP}), which gives rise to voltage-dependent membrane behaviours that are hypothesized to influence rhythmogenesis as well (Koshiya & Smith, 1999; Del Negro *et al.* 2002*a*; Ptak *et al.* 2005; Koizumi & Smith, 2008; but see Del Negro *et al.* 2002*b*, 2005; Pace *et al.* 2007*a*). Finally, since 2001, it has been recognized that inspiratory bursts in preBötC neurons also involve the Ca^{2+}-activated non-specific cation current (I_{CAN}), which can, in some cases, give rise to large-magnitude drive potentials that depolarize preBötC neurons to such an extent that spike-generating currents inactivate, i.e. I_{CAN} can cause intraburst depolarization block (Thoby-Brisson & Ramirez, 2001; Pena *et al.* 2004; Crowder *et al.* 2007; Pace *et al.* 2007*b*; Rubin *et al.* 2009).

Here, we analyse the expression of the membrane properties described above in preBötC neurons with a known genetic background. Given that *Dbx1* expression gives rise to glutamatergic as well as peptidergic and peptide receptor-expressing rhythmogenic neurons in the preBötC, the differences between *Dbx1*$^+$ and *Dbx1*$^-$ neurons may help to reveal the cellular and ionic bases for respiratory rhythmogenesis.

Methods

Neonatal mouse slice preparations

The following protocols have been approved by The College of William & Mary Institutional Animal Care and Use Committee, which operates in accordance to the US National Institutes of Health Office of Laboratory Animal

Welfare, and were performed to conform with the ethical standards as outlined by Drummond (2009). We used transgenic mice that express Cre recombinase fused to the tamoxifen-sensitive estrogen receptor $Dbx1^{+/CreERT2}$ (Hirata *et al.* 2009), floxed reporter mice with inducible expression of the red fluorescent protein variant tdTomato (B6;129S6-$Gt(ROSA)26Sor^{tm9(CAG-tdTomato)Hze}/J$ or $Rosa26^{tdTomato}$, Jax no. 007905; Madisen *et al.* 2010) and floxed reporter mice with inducible expression of enhanced YFP ($Gt(ROSA)26Sor^{tm1(Smo/EYFP)Amc}/J$ or $Rosa26^{EYFP}$, Jax no. 005130). Both the $Dbx1^{+/CreERT2}$ and $Rosa26^{EYFP}$ strains were bred in-house using a CD-1 background strain. The $Rosa26^{tdTomato}$ was maintained as a homozygous line with C57BL/6J background. We verified animal genotype via real-time PCR using primers specific for *Cre*, *EYFP* and *tdRFP* (Transnetyx, Cordova, TN, USA).

Neonatal mice ($n = 83$) were obtained from timed matings of $Dbx1^{+/CreERT2}$ with either $Rosa26^{tdTomato}$ ($n = 69$) or $Rosa26^{EYFP}$ reporter mice ($n = 14$). We visually inspected vaginal plugs to confirm successful mating and induced *Cre* recombination by administering tamoxifen to $Dbx1^{+/CreERT2}$ dams at embryonic day 10.5 (E10.5). If no vaginal plug was detected after 4 days, but the female was judged pregnant by gain of mass and visual signs of abdominal distension, then we utilized a '48 h rule', where we counted 48 h from the start of mating and designated that as E0. In this case, tamoxifen induction of the *Cre* recombinase falls within E9.5–E12.5, during which time *Dbx1* is expressed in hindbrain (Pierani *et al.* 2001; Hirata *et al.* 2009; Gray *et al.* 2010). Tamoxifen (T5648; Sigma Aldrich, St Louis, MO, USA) was dissolved at a concentration of 10 mg ml^{-1} in corn oil and administered by oral gavage to pregnant dams at a concentration of 1 mg (40 g body mass)$^{-1}$.

Neonatal $Dbx1^{+/CreERT2}$; $Rosa26^{tdTomato}$ and $Dbx1^{+/CreERT2}$; $Rosa26^{EYFP}$ mice at postnatal day 0–5 (P0–5) were killed following 4 min of immersion in crushed ice until there was no longer a pinch response from the animals (in compliance with the 2011 guidelines of the Animal Research Advisory Committee, Office of Animal Care and Use, National Institutes of Health, Bethesda, MD, USA). This method renders the animals insentient to the same degree as would occur with gaseous anaesthetics (Danneman & Mandrell, 1997; Fox *et al.* 2007) and facilitates the rapid isolation of the intact brainstem and spinal cord, which would otherwise be damaged if cervical dislocation were used to kill the animals. After the animals were anaesthetized via immersion hypothermia, they were transferred to a dissecting dish and two transections were performed at bregma and the thorax. The neuraxis, from the pons to the lower thoracic spinal cord, was then rapidly removed and further dissected in dish filled with standard artificial cerebrospinal fluid (ACSF) containing (mM): 124 NaCl, 3 KCl, 1.5 $CaCl_2$, 1 $MgSO_4$, 25 $NaHCO_3$, 0.5 NaH_2PO_4 and 30 dextrose, equilibrated with 95% O_2 and 5% CO_2 (pH 7.4). The neuraxis was isolated and pinned onto a paraffin-coated paddle, with its rostral side up and ventral surface facing out. The paddle was fixed into the vice of a vibrating microtome. We cut transverse 550-μm-thick brainstem slices with the preBötC exposed at the rostral face (Ruangkittisakul *et al.* 2011). Slices were then perfused with ACSF at 26–28°C in a recording chamber on a fixed-stage Zeiss Axioskop (Thornwood, NY, USA) with infrared-enhanced differential interference contrast (IR-DIC) imaging and epifluorescence, which enables visual identification and selective recording of target neurons. The K^+ concentration in the ACSF was elevated to 9 mM (standard 9 mM K^+ ACSF) to maintain long-term stability of the preBötC rhythm.

Electrophysiology

Inspiratory-related motor output was recorded from the XII nerve rootlets, which are captured with the preBötC in transverse slices, using suction electrodes and a differential amplifier (Dagan Instruments, Minneapolis, MN, USA). The amplifier gain was set at 2000 and the bandpass filter was set at 300–1000 Hz. The XII discharge was full-wave rectified and smoothed for display. Whole-cell patch-clamp recordings were obtained using patch pipettes with resistance of 4–6 MΩ and a Dagan IX2-700 current-clamp amplifier. The IR-DIC imaging was used to target patch pipettes after fluorescent identification of $Dbx1^+$ neurons. All recordings were digitally acquired at 10 kHz using a PowerLab 16-bit A/D converter after 1 kHz low-pass filtering (AD Instruments, Colorado Springs, CO, USA).

The patch solution contained (mM): 140 potassium gluconate, 10 Hepes, 5 NaCl, 1 $MgCl_2$, 0.1 EGTA, 2 Mg-ATP, 0.3 Na_3-GTP and 2 mg ml^{-1} biocytin (B4261; Sigma Aldrich). We added 50 μM of an Alexa hydrazide dye to the patch solution for fluorescent visualization of the neurons recorded in the whole-cell configuration. Alexa 568 (A10436; Invitrogen, Carlsbad, CA, USA) was used in $Rosa26^{EYFP}$-labelled neurons and Alexa 488 (A10437; Invitrogen) in $Rosa26^{tdTomato}$-labelled neurons.

Current-clamp protocols were performed first in standard 9 mM K^+ ACSF, and then in the presence of a cocktail of ionotropic neurotransmitter receptor antagonists, hereafter called 'blockers' (5 μM picrotoxin, 5 μM strychnine, 10 μM 6-cyano-7-nitroquinoxaline-2, 3-dione and 20 μM DL-2-amino-5-phosphonovalerate) or in a modified low-Ca^{2+}, high-Mg^{2+} ACSF, hereafter called 'low Ca^{2+}'. The low-Ca^{2+} ACSF contained 0.5 mM Ca^{2+} and 2 mM $MgSO_4$. Equimolar substitution of Mg^{2+} for Ca^{2+} ensured that the total concentration of divalent cations remained fixed. We used standard 9 mM K^+ ACSF to record membrane properties of $Dbx1^+$ neurons

in conditions where the respiratory network functions *in vitro* and the synaptic and intrinsic activity can be measured in the context of respiratory rhythm. Then, we added blockers to stop the rhythm and thus measure intrinsic membrane properties in the absence of several common types of ionotropic EPSPs and IPSPs. However, metabotropic receptor-mediated synaptic transmission may still persist in the presence of blockers. Therefore, we used the low-Ca^{2+} ACSF to attain a more complete synaptic isolation of *Dbx1*$^+$ neurons and remeasured intrinsic membrane properties, albeit with the caveat that other biophysical membrane properties, such as Ca^{2+}-dependent K^+ currents, could be affected (Onimaru *et al.* 2003; Zavala-Tecuapetla *et al.* 2008). Nevertheless, low-Ca^{2+} ACSF does not directly affect Na^+-dependent outward currents in preBötC neurons (Del Negro *et al.* 2009; Krey *et al.* 2010). Membrane potential values were not corrected for the liquid junction potential, which measured 1 mV.

We analysed inspiratory drive potentials using the peak parameters plugin in Chart version 7.0 software (AD Instruments). Amplitude and area were measured by digitally smoothing the traces to minimize spikes but preserve the underlying envelope of depolarization of the inspiratory drive potential (Pace *et al.* 2007*a*). Inspiratory drive latency, i.e. burst latency, quantifies the time interval during which a neuron receives temporally summating excitatory synaptic input and may begin to depolarize and discharge spikes, prior to the onset of the XII motor output, which defines the onset of the inspiratory phase *in vitro*. We measured the time interval from the point of first depolarization due to summating EPSPs above baseline membrane potential to the maximal slope of the XII output (Rekling *et al.* 1996*a*; Hayes & Del Negro, 2007). In order to determine the burst latency for any given preBötC neuron, we averaged this interval from at least five consecutive cycles.

Three intrinsic properties (described below) were measured from a baseline membrane potential of −60 mV to provide a uniform standard of comparison among *Dbx1*$^+$ and *Dbx1*$^-$ preBötC neurons. Direct current bias was applied to hold baseline voltage at −60 mV. The membrane time constant (τ_M) was fitted by regression to an exponential function based on the membrane voltage response to a 500 ms hyperpolarizing current pulse. To obtain input resistance (R_N), we applied 1 s current steps in a 10-step sequence. We plotted the resulting voltage–current relationship (*V–I*) and measured its slope in the linear region between (approximately) −95 and −55 mV. To measure the rheobase at a baseline of −60 mV (rheobase$_{-60}$), we applied 12 ms current pulses and manually adjusted the step-current magnitude until it evoked a single spike on the termination of the current pulse at least 50% of the time. The whole-cell capacitance (C_M) was calculated using R_N and τ_M.

We tested for membrane properties indicative of the transient outward current I_A (Rekling *et al.* 1996*a*). We applied suprathreshold 500 ms depolarizing current pulses from baseline membrane potentials of approximately −80 and −50 mV, maintained using direct current bias. The presence of I_A caused a delay of 100–250 ms in spiking activity when the depolarizing current pulse was applied from a holding potential of −80 mV, but no delay in the onset of spiking activity from a holding potential of −50 mV.

We tested for I_h, a mixed cationic current activated by hyperpolarization. We applied 500 ms hyperpolarizing current pulses from a holding potential of −55 mV. The presence of I_h causes a voltage-dependent 'sag' response, wherein the membrane potential trajectory depolarizes back towards the holding potential during the step command (Biel *et al.* 2009).

We compared each parameter measured in *Dbx1*$^+$ and *Dbx1*$^-$ neurons at postnatal ages P0–5. Data were analysed and reported as means ± SEM. Significance was assessed using a two-way ANOVA for data with multiple independent variables. The *F* values from the ANOVAs were reported with the degrees of freedom in parentheses (between groups, within groups). For data with binary classification, we used Fisher's exact test, which is a type of χ^2 test used when a particular category has five or fewer samples. Significance was set at a minimum of $P < 0.05$. Statistical significance is indicated as $^*P < 0.05$ and $^{**}P < 0.01$.

Morphological reconstruction

Slices containing biocytin-loaded neurons were fixed in 4% paraformaldehyde in 0.1 M sodium phosphate buffer for at least 16 h at 4°C. Then, the slices were treated with *Scale* solution containing 4 M urea, 10% (w/v) glycerol and 0.1% (w/v) Triton X-100, for 10 days to clear the tissue and remove opaque background staining (Hama *et al.* 2011). Slices were washed three times for 15 min each in PBS + 1% Triton X-100 and then blocked in 10% heat-inactivated fetal bovine sera (F4135; Sigma Aldrich) for 45 min. Finally, the slices were incubated in fluorescein isothiocyanate-conjugated ExtrAvidin (E2761; Sigma Aldrich) for 2–4 h, rinsed with PBS and coverslipped in Vectashield (H-1500; Vector Laboratories, Burlingame, CA, USA). We visualized recorded neurons using a laser-scanning confocal microscope (Zeiss LSM 510). Images were contrast enhanced and pseudocoloured using the free ImageJ software (National Institutes of Health, Bethesda, MD, USA), and then digitally reconstructed using the freeware Neuromantic reconstruction tool (Myatt *et al.* 2012). The three-dimensional digital reconstructions functioned as tree-like digital objects that we analysed further using the

freeware L-Measure (Scorcioni *et al.* 2008). We compared $Dbx1^+$ and $Dbx1^-$ neuron morphologies according to 39 different measurements and used Student's unpaired *t* tests to compare morphological features between $Dbx1^+$ and $Dbx1^-$ neurons with significance set to a minimum value of $P < 0.05$.

Results

Properties of $Dbx1^+$ and $Dbx1^-$ preBötC neurons measured in the context of respiratory rhythm

To study $Dbx1^+$ neurons, we used brainstem slice preparations from neonatal $Dbx1^{+/CreERT2}$; $Rosa26^{tdTomato}$ ($n = 69$) and $Dbx1^{+/CreERT2}$; $Rosa26^{EYFP}$ ($n = 14$) mice. We visually selected and recorded fluorescent $Dbx1^+$ neurons ($n = 106$) and non-fluorescent $Dbx1^-$ neurons ($n = 42$) in the preBötC, which were dialysed with fluorescent dye to confirm the recording of the intended neuron in each case (Fig. 1*A*–*C*). Inspiratory neurons were identified by depolarizing drive potentials occurring in phase with the XII output. We measured the magnitude of the inspiratory drive potential and the inspiratory drive latency (or burst latency), which quantifies pre-inspiratory activity prior to XII output (see Methods). Baseline membrane potential was -46 ± 1 mV ($n = 76$) for $Dbx1^+$ neurons and -47 ± 1 mV ($n = 42$) for $Dbx1^-$ neurons ($P = 0.6$). Figure 1 displays the rhythmic behaviour of $Dbx1^+$ neurons from EYFP (Fig. 1*A*) and tdTomato (Fig. 1*B*) reporter strains, and a $Dbx1^-$ neuron from the tdTomato strain (Fig. 1*C*), which suggests differences in drive potential characteristics and burst latency. From a baseline membrane potential of −47 mV, the $Dbx1^+$ neuron is active during the interinspiratory burst interval, including during the pre-inspiratory phase, which was observed as early as ∼1 s prior to XII output (Fig. 1*A*, red arrows). Inspiratory bursts all exceed 10 mV in amplitude in this $Dbx1^+$ neuron, and there is some voltage-dependent spike inactivation (i.e. depolarization block) during the inspiratory burst (Fig. 1*A*). In contrast, the $Dbx1^-$ neuron, at a baseline of −49 mV shows a flat voltage trajectory during the interinspiratory burst interval, becomes active immediately prior to XII output, and its inspiratory bursts rarely exceed 10 mV (Fig. 1*C*). Even when a $Dbx1^+$ neuron is held at a hyperpolarized baseline membrane potential (−60 mV) using DC bias, summating synaptic activity is evident during the pre-inspiratory phase several hundred milliseconds prior to XII output. In this case, the lower baseline membrane potential compared with control (not shown) augments the driving force, and the amplitude of the inspiratory drive potential exceeds 20 mV (Fig. 1*B*). Figure 2*A* and *B* illustrates the measurement of the drive potential characteristics and burst latency from a baseline of approximately −50 mV, with XII output, in a $Dbx1^+$ and a $Dbx1^-$ neuron. Given that long burst latency

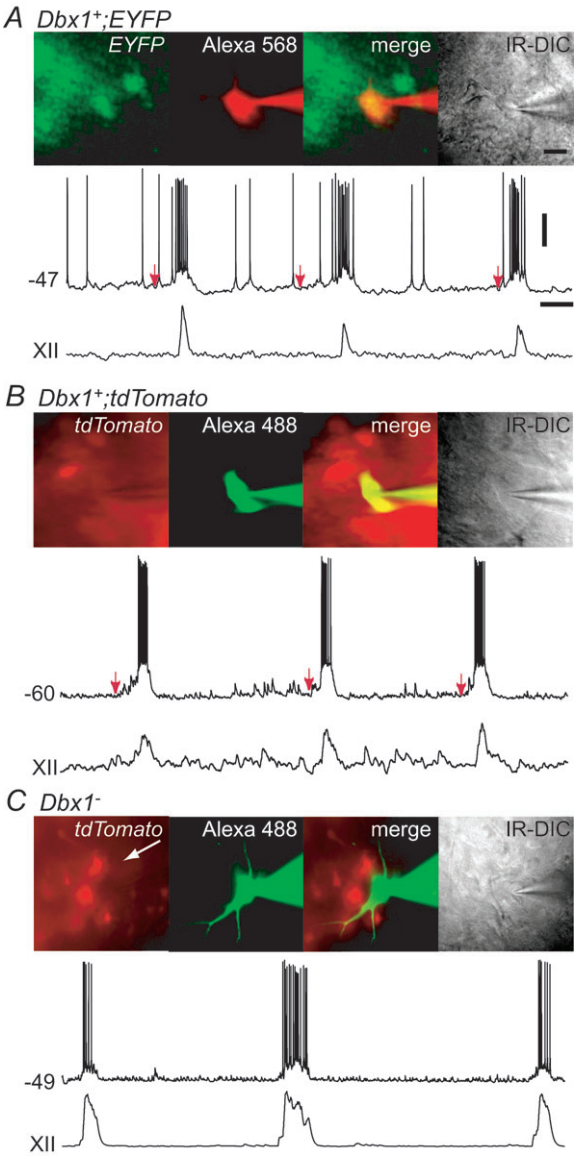

Figure 1. $Dbx1^+$ (*A* and *B*) and $Dbx1^-$ inspiratory neurons (*C*) within the pre-Bötzinger complex (preBötC) of $Dbx1^{+/CreERT2}$; $Rosa26^{EYFP}$ (*A*) or $Dbx1^{+/CreERT2}$; $Rosa26^{tdTomato}$ neonatal mouse slice preparations (*B* and *C*)
A, EYFP-labelled $Dbx1^+$ neuron, Alexa 568-filled, merged fluorescence and infrared-enhanced differential interference contrast (IR-DIC) images with whole-cell recording (top trace) and integrated hypoglossal cranial nerve (XII) output (bottom trace). Red arrows mark the start of the pre-inspiratory phases. *B*, tdTomato-labelled $Dbx1^+$ neuron in a $Dbx1^{+/CreERT2}$; $Rosa26^{tdTomato}$ slice, Alexa 488-filled, merged fluorescence and IR-DIC images with whole-cell recording (top trace) and XII output (bottom trace). *C*, unlabelled $Dbx1^-$ neuron, Alexa 488-filled, merged fluorescence and IR-DIC images with whole-cell recording (top trace) and XII output (bottom trace). Voltage (20 mV) and time (1 s) scale bars apply to all traces. The scale bar (20 μm) shown in the IR-DIC image in *A* applies to all photographs.

(e.g. Fig. 2*A*) accentuates the drive potential area, we additionally assessed drive potential amplitude, which is insensitive to pre-inspiratory timing.

We measured *Dbx1*$^+$ and *Dbx1*$^-$ neurons at P0–5 to determine whether early postnatal development affects rhythmic properties. We used a two-way repeated-measures ANOVA to compare the effect of age on the drive potential characteristics and burst latency between the two groups. There was no significant main effect of age on the drive potential amplitude ($F_{5,100} = 1.6$, $P = 0.17$), drive potential area ($F_{5,100} = 0.6$, $P = 0.69$) or burst latency ($F_{5,83} = 2.2$, $P = 0.057$), so we pooled the data for all postnatal ages (Fig. 2*C–E*).

The main effect of group on the drive amplitude was significant ($F_{1,100} = 9.4$, $P = 0.0028$). The *Dbx1*$^+$ neurons showed larger drive potential amplitude (18.5 ± 0.8 mV, $n = 82$) than *Dbx1*$^-$ neurons (14.4 ± 1.1 mV, $n = 33$). There was also a significant main effect of group on drive potential area ($F_{1,100} = 10.6$, $P = 0.0015$), where *Dbx1*$^+$ neurons showed larger drive potential area (6168 ± 385 mV ms, $n = 82$) than *Dbx1*$^-$ neurons (4036 ± 438 mV ms, $n = 33$). Drive latency was also significantly different between the two groups ($F_{1,83} = 7.6$, $P = 0.0073$), where *Dbx1*$^+$ neurons activated earlier (308 ± 16 ms, $n = 70$) than the *Dbx1*$^-$ neurons (236 ± 15 ms, $n = 28$).

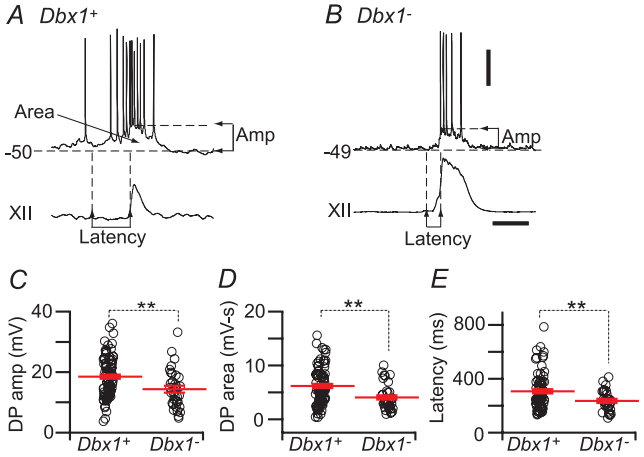

Figure 2. Properties of *Dbx1*$^+$ and *Dbx1*$^-$ neurons measured in the context of respiratory rhythm
A and *B*, top traces, single inspiratory burst in a *Dbx1*$^+$ (*A*) and a *Dbx1*$^-$ neuron (*B*) and the corresponding XII output (bottom traces). Horizontal dashed lines indicate the baseline membrane potential and the amplitude of the depolarization envelope in the burst. Vertical dashed lines indicate: (1) the onset of subthreshold pre-inspiratory depolarization; and (2) the onsets of the inspiratory burst and the XII output. The time interval denotes latency. *C–E*, individual measurements (open circles) of drive potential (DP) amplitude (*C*), drive potential area (*D*) and latency (*E*) of *Dbx1*$^+$ ($n = 82$ for drive potential amplitude and area, $n = 70$ for latency) and *Dbx1*$^-$ neurons ($n = 33$ for drive potential amplitude and area, $n = 28$ for latency). Long red horizontal lines show mean values. Short red lines display SEM. $^{**}P < 0.01$ (two-way repeated measures ANOVA). Voltage (20 mV) and time (0.5 s) scale bars apply to traces in *A* and *B*.

Intrinsic membrane properties

We measured τ_M, R_N, C_M and rheobase$_{-60}$ in standard 9 mM K^+ ACSF in the context of respiratory network activity, and then after silencing the network using a 3 mM K^+ ACSF containing a cocktail of ionotropic receptor antagonists (i.e. blockers) or low-Ca^{2+} ACSF. In each set of conditions, we compared τ_M, R_N and C_M measurements between the *Dbx1*$^+$ and *Dbx1*$^-$ neurons and at the different ages (Fig. 3 and Table 1).

Results of a two-way ANOVA revealed that there was no significant main effect of age or group on the membrane properties τ_M, R_N or C_M over all conditions (Fig. 3; $P > 0.05$), so we pooled the data for all postnatal ages (Table 1). In 9 mM K^+ ACSF, τ_M measured 23 ± 3 ms in both *Dbx1*$^+$ ($n = 26$) and *Dbx1*$^-$ neurons ($n = 17$; $F_{1,32} = 0.02$, $P = 0.89$). The R_N measured 340 ± 34 MΩ ($n = 27$) for *Dbx1*$^+$ and 295 ± 54 MΩ ($n = 17$) for *Dbx1*$^-$ neurons ($F_{1,33} = 0.3$, $P = 0.59$). In *Dbx1*$^+$ neurons, C_M

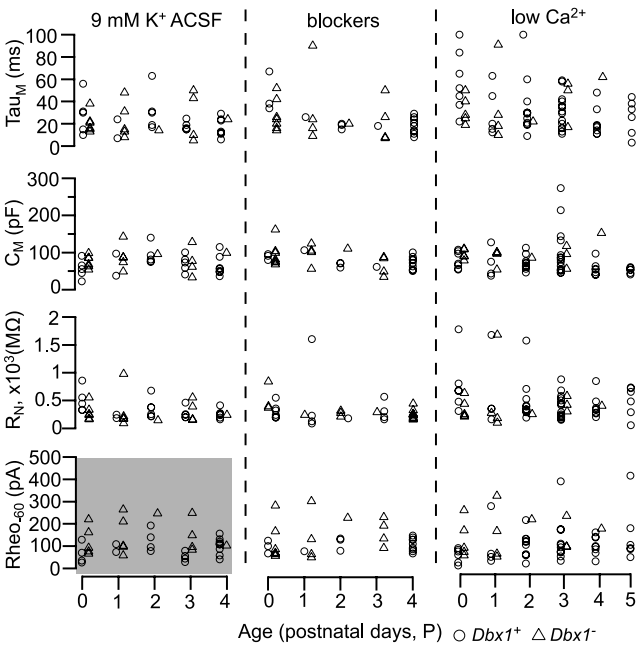

Figure 3. Intrinsic properties of *Dbx1*$^+$ (open circles) and *Dbx1*$^-$ neurons (open triangles) at the different postnatal ages (P0–5)
Membrane time constant (τ_M), input resistance (R_N) and rheobase at −60 mV baseline (Rheo$_{-60}$) were measured in standard 9 mM K^+ artificial cerebrospinal fluid (ACSF; left panel), in the presence of ionotropic receptor antagonists/blockers (middle panel), and in low-Ca^{2+} ACSF (right panel). Whole-cell capacitance (C_M) was computed from τ_M and R_N measurements. Rheobase$_{-60}$ in 9 mM K^+ ACSF was significantly different between *Dbx1*$^+$ and *Dbx1*$^-$ neurons (shaded region in lower left panel). No other measure was statistically significant.

Table 1. Intrinsic membrane properties of *Dbx1*$^+$ and *Dbx1*$^-$ neurons

Treatment	Genotype	τ_M (ms)	R_N (MΩ)	C_M (pF)	Rheo$_{-60}$ (pA)
9 mM K^+ ACSF	*Dbx1*$^+$	23 ± 3 (26)	340 ± 34 (27)	69 ± 5 (26)	87 ± 8* (26)
	Dbx1$^-$	23 ± 3 (17)	295 ± 54 (17)	82 ± 7 (17)	138 ± 18* (16)
Blockers	*Dbx1*$^+$	24 ± 3 (17)	308 ± 38 (17)	75 ± 4 (17)	101 ± 7 (16)
	Dbx1$^-$	28 ± 5 (16)	346 ± 90 (16)	88 ± 8 (16)	134 ± 21 (16)
Low Ca^{2+}	*Dbx1*$^+$	33 ± 3 (54)	499 ± 50 (51)	76 ± 6 (51)	107 ± 12 (46)
	Dbx1$^-$	37 ± 6 (14)	428 ± 105 (14)	95 ± 7 (14)	146 ± 23 (14)

Abbreviations: ACSF, artificial cerebrospinal fluid; C_M, whole-cell capacitance; Rheo$_{-60}$, rheobase at a baseline of −60 mV; R_N, input resistance; τ_M, membrane time constant. Values are means ± SEM. The number of neurons is indicated in parentheses. *$P < 0.05$ (two-way repeated measures ANOVA).

was calculated to be 69 ± 5 pF ($n = 26$), and in *Dbx1*$^-$ neurons C_M was calculated to be 82 ± 7 pF ($n = 17$; $F_{1,32} = 2.0$, $P = 0.17$).

The two-way ANOVA revealed no main effect of age or group on the rheobase$_{-60}$ measured in blockers and low Ca^{2+}. However, there was a significant main effect of group, but not age, for rheobase$_{-60}$ in 9 mM K^+ ACSF. The *Dbx1*$^+$ neurons had a lower rheobase$_{-60}$ (87 ± 8 pA, $n = 26$) than *Dbx1*$^-$ neurons (138 ± 18 pA, $n = 16$; $F_{1,27} = 7.3$, $P = 0.012$; Fig. 3, grey bottom left panel, and Table 1). Rheobase$_{-60}$ was lower for *Dbx1*$^+$ neurons in standard 9 mM K^+ ACSF in the context of network activity, but not when synaptically isolated.

Depolarization block during inspiratory bursts

Large-magnitude drive potentials, which cause depolarization block of spiking during inspiratory bursts, are hypothesized to be a signature feature of the mechanism of rhythmogenesis that amplifies synaptic input in preBötC neurons (Rubin *et al.* 2009). Figure 4 displays *Dbx1*$^+$ (Fig. 4*A* and *B*) and *Dbx1*$^-$ neurons (Fig. 4*C*) that exhibit depolarization block to emphasize that this phenotype was expressed in both groups. Depolarization block during inspiratory bursts may be attributable to I_{CAN}. To test this putative ionic mechanism, we selectively recorded from four *Dbx1*$^+$ neurons showing drive potential ≥20 mV, three of which exhibited depolarization block. We previously demonstrated that flufenamic acid (FFA), which reduces but does not completely block I_{CAN} at 100 μM, attenuates inspiratory drive potentials by ∼40% in preBötC neurons (Pace *et al.* 2007*b*). Likewise, in *Dbx1*$^+$ neurons, bath application of FFA (100 μM) reduced the mean drive potential amplitude by 42%, from 30.3 ± 4.0 to 17.6 ± 4.0 mV ($n = 4$; Fig. 4*D*, all symbols). In the subset of *Dbx1*$^+$ neurons showing depolarization block ($n = 3$), 100 μM FFA abolished the depolarization block in two cases (Fig. 4*A* and *D*, filled circles). In the third neuron, FFA did not abolish the depolarization block, although the magnitude of the drive potential was attenuated by 22% (Fig. 4*B* and *D*, open triangles). In the *Dbx1*$^+$ neuron that did not show depolarization block, the drive potential was attenuated by 48% (Fig. 4*D*, open squares). These data reaffirm that I_{CAN} contributes to inspiratory burst generation and provide experimental evidence suggesting that I_{CAN} contributes substantially to depolarization block. However, I_{CAN} is not the only ionic mechanism underlying depolarizing block; non-I_{CAN} mechanisms may contribute measurably, especially in the case of extremely large-magnitude inspiratory bursts (e.g. Fig. 4*B*). We observed a total of 41 neurons (both *Dbx1*$^+$ and *Dbx1*$^-$) that exhibited depolarization block; however, depolarization block was more common in *Dbx1*$^+$ neurons. Thirty-five of 95 (37%) *Dbx1*$^+$ neurons and six of 42 *Dbx1*$^-$ neurons (14%) exhibited depolarization block in more than half of their inspiratory burst cycles, which was a statistically significant difference (Fig. 4*E*; Fisher's exact test, $P = 0.0085$).

Voltage-dependent bursting properties

We performed rudimentary tests for voltage-dependent bursting properties attributable to coexpression of I_{NaP} and non-gated leak K^+ current in the appropriate ratio (Del Negro *et al.* 2002*a*; Koizumi & Smith, 2008). We adjusted the baseline membrane potential to between −55 and −45 mV and then observed whether 'ectopic' bursting emerged in the intervals between XII bursts. This rudimentary test for voltage-dependent pacemaker properties is unsophisticated but nonetheless quite reliable (Del Negro *et al.* 2001, 2002*a*,*b*, 2005; Thoby-Brisson & Ramirez, 2001; Pena *et al.* 2004). Example traces show inspiratory and 'ectopic' bursts of *Dbx1*$^+$ (Fig. 5*A*) and *Dbx1*$^-$ neurons (Fig. 5*B*). Ectopic bursts that occur between inspiratory cycles of XII output, when the baseline membrane potential is biased to the activation threshold of I_{NaP} (approximately −55 mV), are a reliable indicator of voltage-dependent bursting properties (Smith *et al.* 1991; Thoby-Brisson & Ramirez, 2001; Del Negro *et al.* 2002*b*, 2005). At baseline voltages below its activation threshold, I_{NaP} remains deactivated, and ectopic bursts do not occur. Seventeen of 91 (19%) *Dbx1*$^+$ neurons and seven of 42 *Dbx1*$^-$ neurons (17%) exhibited ectopic bursting at membrane potentials above −55 mV, whereas burst activity for both groups was confined to the inspiratory

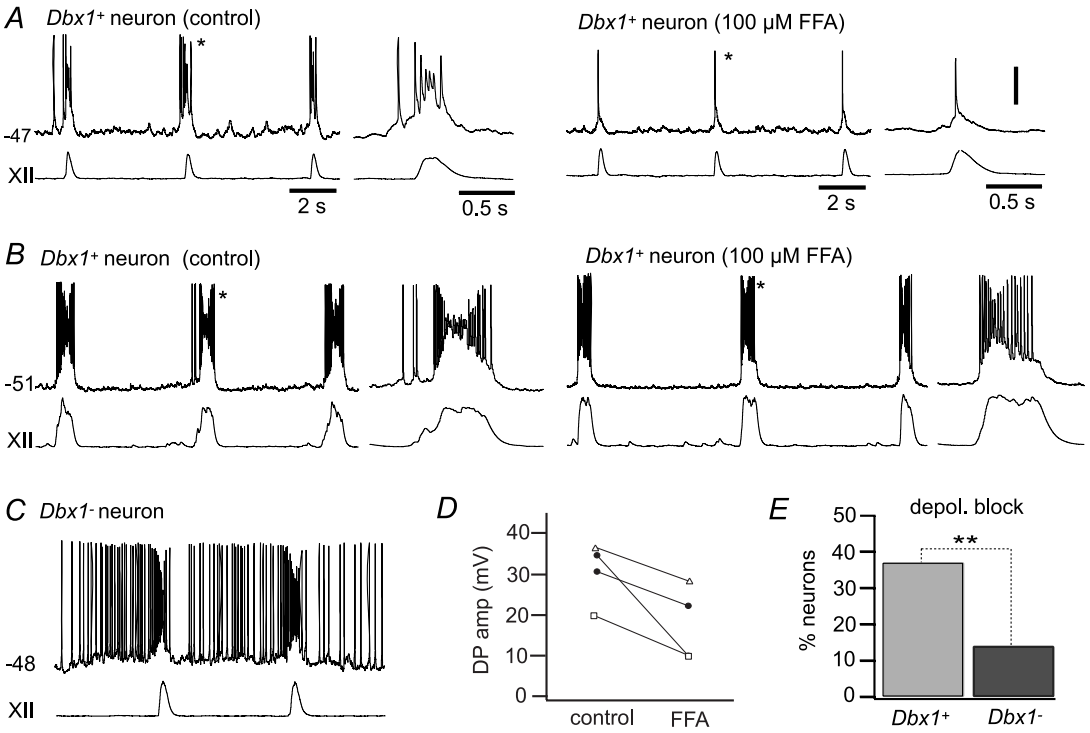

Figure 4. Intraburst depolarization block in *Dbx1*$^+$ and *Dbx1*$^-$ neurons
A and *B*, two example *Dbx1*$^+$ neurons exhibiting depolarization block during inspiratory bursts in standard 9 mM K^+ ACSF (control) and their bursts after bath application of 100 μM flufenamic acid (FFA). Baseline membrane potential reflects zero applied current. *C*, *Dbx1*$^-$ neuron exhibiting depolarization block during an inspiratory burst. *D*, drive potential amplitudes in four *Dbx1*$^+$ neurons in control conditions and in the presence of 100 μM FFA. All four neurons exhibited a decrease in the drive potential amplitude upon bath application of 100 μM FFA. Depolarization block was eliminated by FFA application in two neurons (filled circles), whereas depolarization block persisted after FFA application in one neuron (open triangles, neuron in *B*). A *Dbx1*$^+$ neuron with no depolarization block in control conditions also showed a reduction in drive potential amplitude in the presence of FFA (open squares). *E*, percentage of *Dbx1*$^+$ ($n = 95$) and *Dbx1*$^-$ neurons ($n = 42$) exhibiting intraburst depolarization. Vertical scale bar in *A* (20 mV) applies to all traces. Separate time scale bars are given for main traces in *A*–*C* as well as the single-burst insets in *A* and *B* only. $^{**}P < 0.01$ (Fisher's exact test).

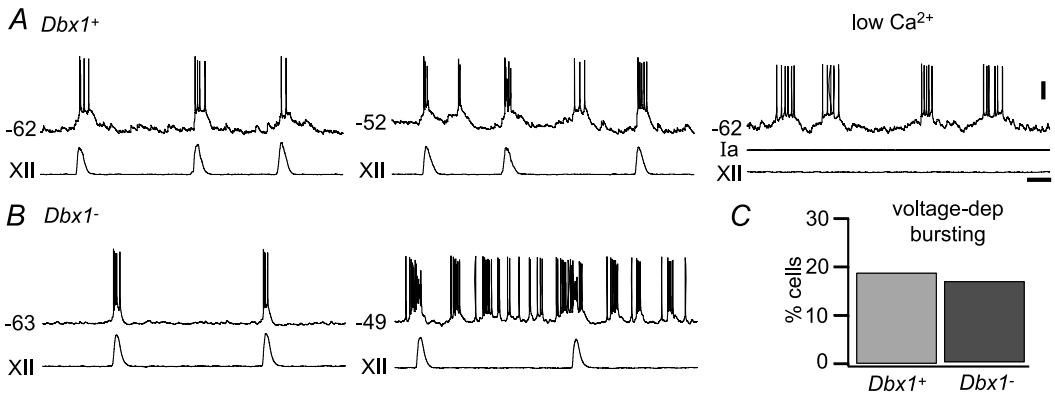

Figure 5. Voltage-dependent bursting properties in *Dbx1*$^+$ and *Dbx1*$^-$ neurons
A, a *Dbx1*$^+$ neuron showing inspiratory bursts at a baseline membrane potential of −62 mV (left), ectopic voltage-dependent bursts at a more depolarized membrane potential of −52 mV (centre) and in low-Ca^{2+} conditions (right). I_a refers to applied current to demonstrate that bursting is intrinsic after the network activity stops (i.e. no XII output). *B*, inspiratory bursts and XII output in a *Dbx1*$^-$ neuron (left) and ectopic voltage-dependent bursts at more depolarized membrane potential (right). *C*, percentage of neurons with voltage-dependent bursting properties in a sample size of 91 *Dbx1*$^+$ and 42 *Dbx1*$^-$ neurons in the preBötC. Voltage (20 mV) and time (1 s) scale bars apply to all traces.

cycles at membrane potentials less than −60 mV. We confirmed the voltage-dependent bursting properties by synaptically isolating 12 *Dbx1*$^+$ neurons that showed ectopic bursts. All continued bursting after application of blockers or low-Ca^{2+} ACSF (Fig. 5*A*, right). The relative expression of voltage-dependent bursting activity in *Dbx1*$^+$ *versus* *Dbx1*$^-$ neurons was not significantly different (Fisher's exact test, $P = 1$; Fig. 5*C*).

Relative expression of delayed excitation and 'sag' potentials

It has been proposed that preBötC neurons that express I_A, but lack I_h, are of primary importance for rhythmogenesis (Rekling *et al.* 1996*a*; Gray *et al.* 1999). These peptide-sensitive neurons were dubbed 'type 1' to indicate their putative importance. Neurons that express I_h but not I_A, and were shown to be less sensitive to neuropeptides, were proposed to activate downstream from type 1 neurons; hence, this second phenotype was dubbed 'type 2' (Rekling *et al.* 1996*a*,*b*; Gray *et al.* 1999). We evaluated this classification scheme in *Dbx1*$^+$ and *Dbx1*$^-$ neurons in 9 mM K^+ ACSF and in low-Ca^{2+} conditions.

We performed basic tests for delayed excitation indicative of I_A. Twenty-seven of 48 *Dbx1*$^+$ neurons tested exhibited a 100–250 ms delay in the onset of spiking activity in response to a suprathreshold current step from a holding potential of approximately −80 mV (e.g. Fig. 6*A*). During this delay, the neurons exhibited a depolarizing ramp-like voltage trajectory, which suggests the slow inactivation of I_A (Hayes & Del Negro, 2007). After adjusting DC bias, we injected the same net current during the 500 ms current step, but observed no delay in the onset of spiking from a baseline of −50 mV. In contrast, 21 of 48 *Dbx1*$^+$ (Fig. 6*B*) and 12 of 16 *Dbx1*$^-$ neurons (Fig. 6*C*) showed no delay in the onset of spiking activity in response to 500 ms depolarizing current steps from a holding potential of −80 mV. The spike rate in these neurons (Fig. 6*B* and *C*) peaked at the onset of the current step and tended to accommodate thereafter for the remainder of the current stimulus; nor was there a delay in the onset of spiking in these *Dbx1*$^+$ and *Dbx1*$^-$ neurons in response to the same net current from a holding potential of −50 mV (Fig. 6*B* and *C*).

The presence of I_h causes a depolarizing 'sag' in the membrane potential trajectory in response to a sustained hyperpolarizing step current (Biel *et al.* 2009). Twenty of 27 *Dbx1*$^+$ neurons that expressed I_A did not exhibit such a sag response (Fig. 6*A*). In contrast, there was a >10 mV sag response in 17 of 21 *Dbx1*$^+$ (Fig. 6*B*) and eight of 12 *Dbx1*$^-$ neurons (Fig. 6*C*) that did not express I_A. Neurons that expressed sag potentials often exhibited postinhibitory rebound at the end of the current pulse (Fig. 6*B*), which could be attributed to slow deactivation of I_h or possibly the de-inactivation of a low-voltage-activated Ca^{2+} current (Elsen & Ramirez, 2005).

The expression of I_A and I_h showed a statistically significant tendency to be mutually exclusive in *Dbx1*$^+$ neurons, as suggested by the type 1 *versus* type 2 classification scheme (Rekling *et al.* 1996*a*,*b*; Gray *et al.* 1999). The *Dbx1*$^+$ neurons exhibited delayed excitation without sag (type 1; Fig. 6*A*) or sag without delayed excitation (type 2; Fig. 6*B*) in comparable proportions (42%, 20 of 48 tested, and 35%, 17 of 48 tested; Table 2). Type 1 and type 2 *Dbx1*$^+$ phenotypes, as defined by mutually exclusive expression of I_A and I_h, occur at significantly higher frequency than the two other possible 'types', namely delayed excitation and sag both present (15%, 7 of 48 tested; Table 2) or delayed excitation and sag both absent (8%, 4 of 48 tested; Table 2; Fisher's exact test, $P = 0.0004$). The *Dbx1*$^-$ neurons (Fig. 6*C*) generally expressed the type 2 phenotype (50%, 8 of 16 tested; Table 2). However, the other combinations, including type 1 (12.5%, 2 of 16 tested; Table 2), delayed excitation

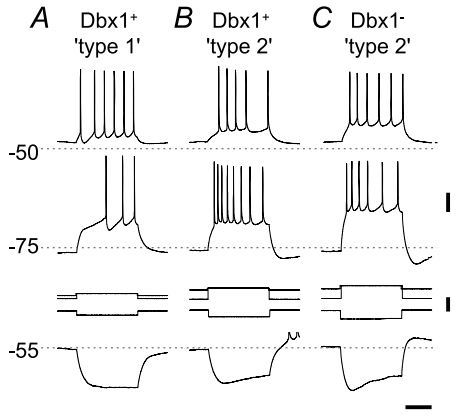

Figure 6. Delayed excitation and 'sag' potentials in *Dbx1*$^+$ (*A* and *B*) and *Dbx1*$^-$ neurons (*C*)
Depolarizing pulses (500 ms) were injected from a depolarized potential (above −50 mV) and from a hyperpolarized potential of −75 mV. Hyperpolarizing pulses were injected from −55 mV. *A*, a type 1 *Dbx1*$^+$ neuron exhibiting delayed excitation from −75 mV, but not from −50 mV, and no sag potential in response to the hyperpolarizing pulse. *B* and *C*, a type 2 *Dbx1*$^+$ (*B*) and a *Dbx1*$^-$ neuron (*C*) exhibiting sag potentials but no delayed excitation. Spikes are truncated above −50 mV in *B* (bottom trace). Voltage (20 mV), current (0.2 nA) and time (0.2 s) scale bars apply to all traces.

Table 2. Expression of delayed excitation and sag potential in *Dbx1*$^+$ and *Dbx1*$^-$ neurons

	Dbx1$^+$ ($n = 48$)		*Dbx1*$^-$ ($n = 16$)	
Characteristic	Sag	No sag	Sag	No sag
Delayed excitation	7 (15%)	20 (42%)	2 (12.5%)	2 (12.5%)
No delayed excitation	17 (35%)	4 (8%)	8 (50%)	4 (25%)

and sag both present (12.5%, 2 of 16 tested; Table 2) and finally delayed excitation and sag both absent (25%, 4 of 16 tested; Table 2), were observed at commensurate frequencies, so the relative prevalence of type 2 among *Dbx1*$^-$ neurons did not rise to statistical significance (Fisher's exact test, $P = 0.24$).

Morphological properties

We imaged 23 *Dbx1*$^+$ and 14 *Dbx1*$^-$ biocytin-filled inspiratory neurons (Fig. 7*A*, *B*), and then performed three-dimensional digital reconstruction in 14 *Dbx1*$^+$ and 12 *Dbx1*$^-$ neurons (Figs 8*A*–*F* and 9*A*–*F*). Digital reconstructions have been added to the public domain via the NeuroMorpho.org database. There were no noticeable differences in the soma shape of the *Dbx1*$^+$ and *Dbx1*$^-$ neurons, which appeared fusiform or triangular in contour. The *Dbx1*$^+$ and *Dbx1*$^-$ neurons were not significantly different in surface area measurements. The *Dbx1*$^+$ neurons measured $561 \pm 48\ \mu m^2$ in soma surface area and $4008 \pm 634\ \mu m^2$ in total somatodendritic surface area, whereas *Dbx1*$^-$ neurons measured 672 ± 59 and $4769 \pm 452\ \mu m^2$, respectively (Student's unpaired *t* test, $P = 0.16$ and $P = 0.34$, respectively).

The dorsoventral span of dendrites measured on average $269 \pm 38\ \mu m$ in *Dbx1*$^+$ neurons and $247 \pm 21\ \mu m$ in *Dbx1*$^-$ neurons, which was not significantly different (*t* test, $P = 0.61$). The average mediolateral span was also comparable between the two groups ($287 \pm 38\ \mu m$ in *Dbx1*$^+$ *versus* $292 \pm 43\ \mu m$ in *Dbx1*$^-$, *t* test, $P = 0.94$; Fig. 8). Although *Dbx1*$^+$ and *Dbx1*$^-$ neurons did not appear to differ in size as measured in dorsoventral or mediolateral orientations, the same was not true for projection in the parasagittal plane. The dendrites of the *Dbx1*$^-$ neurons extended deeper in the rostrocaudal axis, with a total average depth of $54 \pm 4\ \mu m$, compared with an average total depth of $37 \pm 4\ \mu m$ for *Dbx1*$^+$ neurons (*t* test, $P = 0.0071$; Fig. 9).

The *Dbx1*$^-$ neurons appeared to have more branches (42 ± 8) than *Dbx1*$^+$ neurons (26 ± 4). The maximal branch order from the soma (soma is order 0; a branch that originates from the soma is order 1; second bifurcation from the same branch is order 2, and so on) was 8 ± 2 in *Dbx1*$^-$ neurons compared with 4 ± 0.4 in *Dbx1*$^+$ neurons. However, even though the number of branches and branch order differed by approximately 2-fold (Figs 7 and 8), these differences did not reach statistical significance (*t* tests, $P = 0.08$).

The dendrites of the 23 *Dbx1*$^+$ neurons did not exhibit spines (Figs 7*A* and *C* and 8*A*–*C*) whereas three of 14 *Dbx1*$^-$ neurons (21%) showed spines and protrusions (Figs 7*B* and *C* and 8*D*–*F*). This difference in the expression (or lack) of dendritic spines and protrusions was statistically significant (Fig. 7*C*; Fisher's exact test, $P = 0.047$).

Eleven of 23 *Dbx1*$^+$ neurons (48%) projected axons towards ($n = 10$) or across the mid-line ($n = 1$; Fig. 8*A*–*C*). Two of the 14 (14%) *Dbx1*$^-$ neurons had axons projecting towards, yet none crossing, the mid-line (Fig. 8*D*–*F*). In many cases, the axons of *Dbx1*$^-$ neurons appeared to be severed at the rostral face of the slice, suggesting a rostral projection path ($n = 9$ of 14 *Dbx1*$^-$ neurons reconstructed). The severed axon was identified by a bleb, significantly larger in diameter than its parent axon, at the immediate rostral surface of the slice preparation. Nonetheless, the relative fraction of neurons with contralateral projections did not rise to statistical significance (Fisher's exact test, $P = 0.0740$).

Discussion

The *Dbx1*$^+$ neurons are putatively an essential respiratory rhythmogenic population and the predominant source of glutamatergic interneurons in the ventrolateral medulla, including the preBötC (Bouvier *et al.* 2010; Gray *et al.* 2010). A comparative analysis of inspiratory *Dbx1*$^+$ and *Dbx1*$^-$ neurons in the preBötC may help to elucidate the cellular mechanisms of rhythm generation. The

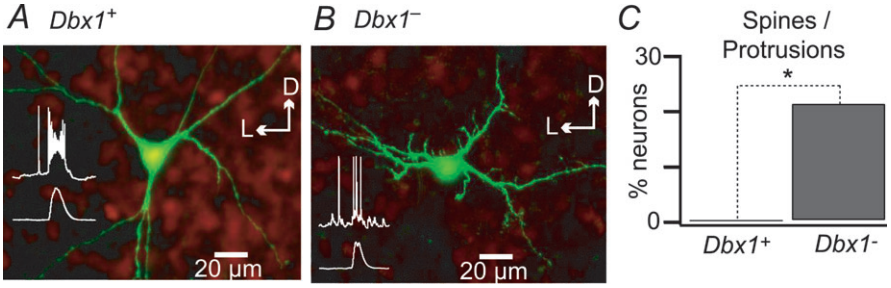

Figure 7. Morphological characteristics of *Dbx1*$^+$ and *Dbx1*$^-$ neurons
A and *B*, confocal images of biocytin-filled neurons processed with fluorescein isothiocyanate-conjugated ExtrAvidin. *Dbx1*$^+$ (*A*) and *Dbx1*$^-$ neuron (*B*) in a *Dbx1*$^{+/CreERT2}$; *Rosa26*^{tdTomato} and a representative inspiratory burst and XII output (insets). *C*, bar graph showing the percentage of *Dbx1*$^+$ ($n = 23$) and *Dbx1*$^-$ neurons ($n = 14$) with dendritic spines/protrusions. $^*P < 0.05$ (Student's unpaired t test). Dorsal and lateral orientation are indicated via arrows labeled D and L.

Dbx1$^+$ neurons differ from *Dbx1*$^-$ neurons mainly on the basis of properties measurable in the context of respiratory network activity, including larger inspiratory burst magnitude and longer burst latency. We used current-clamp protocols to infer the expression of I_h and I_A (Thoby-Brisson *et al.* 2000; Hayes *et al.* 2008). The *Dbx1*$^+$ neurons tend to express I_A with no detectable I_h, or I_h with no detectable I_A, whereas the *Dbx1*$^-$ neurons show no consistent expression patterns. The *Dbx1*$^+$ neuron dendrites are smooth (spineless) and largely confined to the transverse plane, whereas the *Dbx1*$^-$ neuron dendrites in some cases show spines and protrusions, and in general span a greater range of the parasagittal plane. We propose that intrinsic conductances evoked in the context of network activity and dendritic properties differentiate *Dbx1*$^+$ and *Dbx1*$^-$ neurons in the preBötC and thus could explain, at least in part, the presumably rhythm-generating function of *Dbx1*$^+$ neurons.

The *Dbx1*$^+$ neurons show a longer inspiratory drive latency than the *Dbx1*$^-$ neurons and thus may provide the 'on' switch of inspiration. However, *Dbx1*$^-$ neurons also activate prior to XII motor output, and the difference in inspiratory drive latency, while statistically significant, is merely 72 ms. This property of early drive latency is consistent with the pre-inspiratory activity reported for putatively respiratory rhythmogenic neurons that were not identified by transmitter phenotype or genotype, but nonetheless showed drive latency of ∼400 ms and were characterized by expression of I_A and neuropeptide sensitivity, but lack of I_h (Rekling *et al.* 1996*a*,*b*). Furthermore, pre-inspiratory activity due to recurrent synaptic excitation has been proposed to be a key rhythmogenic feature based on intracellular studies *in vivo* and *in vitro* for 30 years (Richter, 1982; Ezure, 1990; Bianchi *et al.* 1995; Schwarzacher *et al.* 1995; Richter & Spyer, 2001; Feldman & Del Negro, 2006).

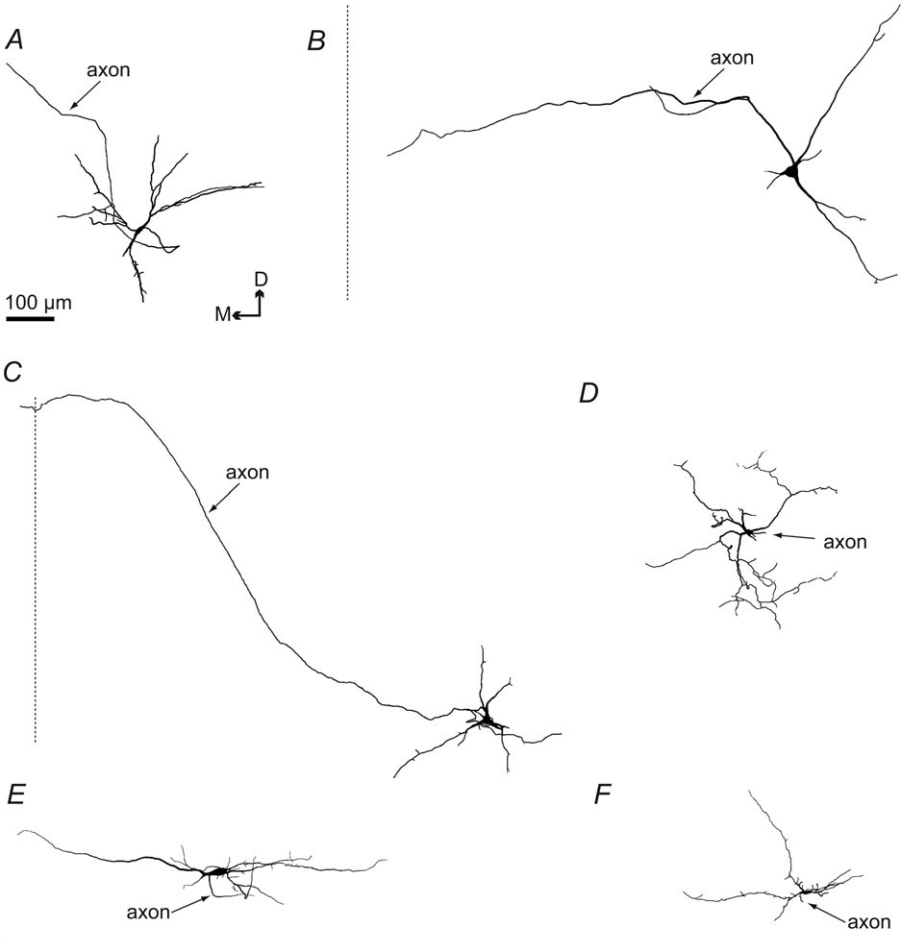

Figure 8. Digital reconstruction of *Dbx1*$^+$ (*A–C*) and *Dbx1*$^-$ neurons (*D–F*) in the transverse plane, with axons indicated
A–C, *Dbx1*$^+$ neurons ($n = 14$) with axons that project towards the mid-line of the slice preparation (shown with a dotted line). The axon of one *Dbx1*$^+$ neuron (*C*) crossed the mid-line of the slice. *D–F*, *Dbx1*$^-$ neurons ($n = 12$) with axons that project short distances before truncation. Dorsomedial orientation is indicated. Scale bar applies to *A–F*.

The *Dbx1*$^+$ neurons show significantly larger magnitude inspiratory drive potentials than the *Dbx1*$^-$ neurons. Moreover, a significantly greater number of *Dbx1*$^+$ neurons exhibit intraburst depolarization block, which is hypothesized to be a signature feature of the rhythmogenic mechanism that amplifies excitatory synaptic input. The ionic mechanism underlying the larger inspiratory bursts and depolarization block, in particular, cannot be determined with certainty from the present study. Nevertheless, the recruitment of I_{CAN} is proposed to be important for inspiratory burst generation (Thoby-Brisson & Ramirez, 2001; Pena *et al.* 2004; Del Negro *et al.* 2005; Ramirez & Viemari, 2005; Ramirez *et al.* 2011). Early drive latency and large burst magnitude may be attributable, at least in part, to recurrent synaptic excitation convolved with I_{CAN} expression in *Dbx1*$^+$ neurons, although other non-I_{CAN} ionic mechanisms, which may include I_{NaP} as well as heretofore unrecognized intrinsic currents, cannot be ruled out (e.g. Fig. 4*B*). The interaction of synaptic input coupled to postsynaptic intrinsic conductances, including (but not limited to) I_{CAN}, may be part of the principal rhythm-generating mechanism, because it is significantly different in *Dbx1*$^+$ compared with *Dbx1*$^-$ neurons of the preBötC, and leads to greater magnitude inspiratory drive potentials. A critical area for future investigation is to measure the biophysical properties of the intrinsic currents (such as I_{CAN} and I_{NaP}, as well as unrecognized novel non-I_{CAN} currents) that amplify synaptic input, to understand the inception of inspiratory drive potential in *Dbx1*$^+$ neurons of the preBötC.

Pre-Bötzinger complex neurons that express I_A but lack I_h (dubbed type 1) were hypothesized to be primary rhythm generators based on their early drive latency (i.e. pre-inspiratory activity) and sensitivity to neuropeptide modulation. Pre-Bötzinger complex neurons that express I_h but not I_A (dubbed type 2) were proposed to activate downstream from type 1 neurons (Rekling *et al.*

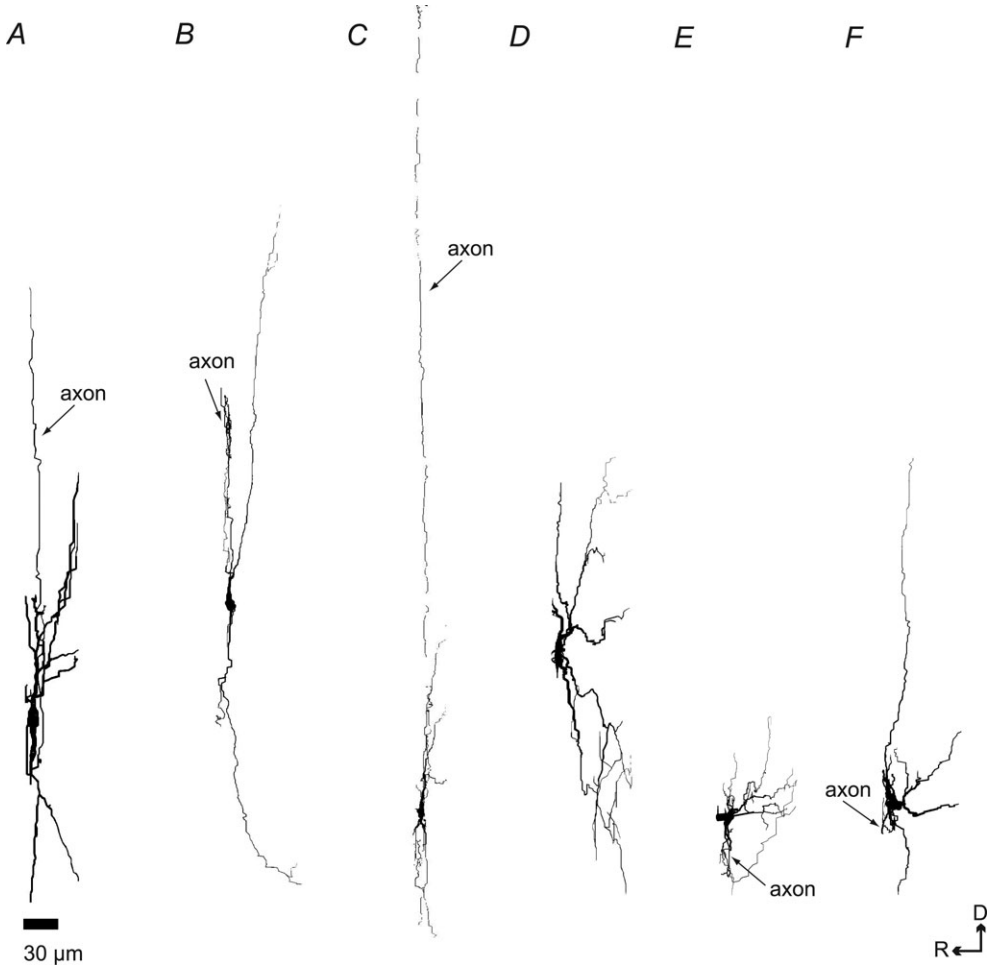

Figure 9. Digital reconstruction of *Dbx1*$^+$ (*A–C*) and *Dbx1*$^-$ neurons (*D–F*) in the parasagittal plane, with axons indicated
A–C, *Dbx1*$^+$ neurons. *D–F*, *Dbx1*$^-$ neurons with projections that span the rostrocaudal axis to a greater extent than *Dbx1*$^+$ neurons. Abbreviations: D, dorsal; and R, rostral. Scale bar applies to *A–F*.

1996*a*,*b*; Gray *et al.* 1999; Hayes & Del Negro, 2007), and thus could serve a rhythmogenic or premotor role. A strict classification of type 2 preBötC neurons as premotor is questionable, because blockade of I_h modulates respiratory frequency, which suggests that a subpopulation of type 2 neurons are integrated into the mechanism of rhythm generation (Thoby-Brisson *et al.* 2000). A premotor role for type 2 neurons notwithstanding, it seems likely that type 1 and type 2 preBötC neurons both serve in a rhythmogenic capacity. The *Dbx1*$^+$ neurons expressed I_A and I_h with a significant trend towards mutual exclusivity, consistent with the classification scheme in the study by Rekling *et al* (1996). The *Dbx1*$^+$ neurons belonged to either the type 1 or type 2 group in roughly equal numbers, and infrequently expressed I_A and I_h together or lacked expression of both. In contrast, *Dbx1*$^-$ neurons showed no consistent relationship regarding I_A and I_h expression, even though 50% were type 2.

Why might the *Dbx1*$^+$ type 1 phenotype be rhythmogenic? The often complementary expression of I_A without I_h could be important for rhythmogenesis if these expression patterns apply to dendrites. We previously measured somatic I_A in outside-out patches and proposed that this intrinsic current prevents recurrent excitatory input from causing the membrane potential to cross spike threshold prematurely during the pre-inspiratory phase (Hayes *et al.* 2008). If I_A is expressed in *Dbx1*$^+$ neuron dendrites, then it could likewise activate at or above threshold to prevent spurious dendritic plateau depolarizations, as previously shown in CA1 pyramidal neuron dendrites (Hoffman *et al.* 1997; Acker & White, 2007). In contrast, in CA1 neuron dendrites, I_h limits subthreshold temporal summation, allowing proximal and distal inputs to produce the same temporal output patterns (Magee, 1999; Migliore *et al.* 2004). Therefore, it may be desirable to preclude I_h expression in *Dbx1*$^+$ interneurons of the preBötC to promote temporal summation of subthreshold inputs in dendrites. We propose that the presence of I_A and lack of I_h may prevent spurious burst discharge and yet promote temporal summation in type 1 *Dbx1*$^+$ neurons during the pre-inspiratory interval. However, this remains to be tested fully by direct recordings in dendrites and via computer simulation.

Type 2 neurons were proposed to activate downstream from type 1 neurons (Rekling *et al.* 1996*a*), and in that regard may play a premotor role in respiratory network activity. However, blocking I_h in type 2 neurons significantly boosts collective activity in XII motoneurons and increases respiratory frequency, which indicates that type 2 neurons have a direct role in rhythm generation as well as premotor drive transmission (Thoby-Brisson *et al.* 2000). With respect to rhythmogenesis, type 2-like inspiratory neurons are proposed to modulate respiratory frequency. Whether I_h acts as a leak current or influences dendritic synaptic integration in a previously unrecognized manner remains to be determined (Thoby-Brisson *et al.* 2000). With respect to a premotor role, *Dbx1*$^+$ neurons are found in a continuous dorsomedial-to-ventrolateral line in the transverse plane (Bouvier *et al.* 2010; Gray *et al.* 2010), which covers the intermediate region between the preBötC and the XII nucleus containing respiratory premotor neurons (Koizumi *et al.* 2008; Volgin *et al.* 2008). Therefore, type 2 *Dbx1*$^+$ neurons may participate in an oligosynaptic premotor pathway from rhythmogenic preBötC neurons to XII motoneurons, but this remains to be demonstrated.

One-fifth (i.e. 20%) of all neurons in the preBötC, including *Dbx1*$^+$ glutamatergic neurons (present study), glycinergic neurons (Morgado-Valle *et al.* 2010), and the neurokinin-1 receptor-expressing population (Pagliardini *et al.* 2005) that overlaps with *Dbx1*$^+$ neurons, express voltage-dependent bursting properties. Although expression of I_{NaP} in the preBötC is higher than in adjacent regions of the medulla (Ptak *et al.* 2005; Koizumi & Smith, 2008), voltage-dependent bursting does not differentiate the critical *Dbx1*$^+$ population from the *Dbx1*$^-$ population, and thus we conclude that voltage-dependent bursting properties are less likely to constitute a key rhythmogenic feature of *Dbx1*$^+$ neurons. Our identification of voltage-dependent pacemaker properties in *Dbx1*$^+$ and *Dbx1*$^-$ neurons in the preBötC is unlikely to detect I_{CAN}-dependent pacemaker properties, which are far less voltage dependent (Pena *et al.* 2004; Del Negro *et al.* 2005; Ramirez *et al.* 2011), and thus unlikely to be recognized via ectopic bursting. Nevertheless, I_{CAN}-dependent pacemaker neurons are extremely rare at P0–5 (Pena *et al.* 2004; Del Negro *et al.* 2005), so the deficiencies of the screening protocol are unlikely to affect the relative prevalence of pacemaker activity characterized in *Dbx1*$^+$ *versus Dbx1*$^-$ neurons.

The *Dbx1*$^+$ neurons are identical in basic membrane properties (τ_M, R_N and C_M) to *Dbx1*$^-$ neurons, but have lower rheobase$_{-60}$ in the context of network activity. The *Dbx1*$^+$ neurons may be 'primed' by ongoing synaptic activity acting via metabotropic receptors and intracellular signalling, which would enhance excitability and facilitate spike discharge, resulting in a lower threshold and rheobase. However, in type-1-like *Dbx1*$^+$ neurons, the lower rheobase may be mitigated by expression of I_A. If the role of I_A is to provide an appropriate delay for the onset of plateau-like depolarization in support of inspiratory burst generation, then a lower rheobase may be important to ensure robust spiking at the onset of, and during, inspiratory bursts.

We identified axon projections of *Dbx1*$^+$ neurons that either crossed or approached the mid-line, which is consistent with the previous finding that *Dbx1*$^+$ interneurons are commissural and bilaterally synchronize the preBötC (Bouvier *et al.* 2010). Some *Dbx1*$^-$ neurons

showed contralateral projections, but most did not. In many instances, the lack of contralateral projections reflects axotomy due to transverse slicing. A number of *Dbx1*$^-$ neurons appear to have axons projecting rostrally, which may indicate communication with rostral respiratory nuclei, such as the Bötzinger complex or the retrotrapezoid nucleus/parafacial respiratory group. In that regard, we speculate that the inspiratory bursts of *Dbx1*$^-$ neurons provide a faithful mimic of inspiratory burst activity in *Dbx1*$^+$ neurons that is communicated via rostrally projecting axons to influence or possibly inhibit other respiratory-related nuclei outside the preBötC. If so, then *Dbx1*$^-$ neurons could play a role in co-ordinating inspiratory as well as expiratory motor outputs.

The *Dbx1*$^+$ neurons have dendrites largely confined to the transverse plane, which may facilitate local synaptic integration among the bilaterally projecting *Dbx1*$^+$ subpopulation. The *Dbx1*$^-$ neurons extend their dendritic arbor outside the plane of section, deeper in the rostrocaudal axis by $\sim$17 μm. This difference, while statistically significant, is rather small and suggests that *Dbx1*$^-$ neurons also project predominantly in the transverse plane. Therefore, *Dbx1*$^-$ neurons may also be optimized for synaptic integration locally in the preBötC, while simultaneously their slightly deeper dendritic projections may facilitate synaptic integration from other respiratory sites in the caudal medulla. Furthermore, because their axons were often severed in a rostral trajectory ($n = 9$ of 14 *Dbx1*$^-$ neurons reconstructed), we speculate that *Dbx1*$^-$ neurons may preferentially project to rostral respiratory circuits.

The *Dbx1*$^+$ neurons have a tendency for fewer branches with no spines, whereas $\sim$20% of *Dbx1*$^-$ neurons show spines and protrusions. Smooth, unbranched dendrites in *Dbx1*$^+$ neurons may promote signal conduction, which would help to retain the amplitude of synaptic input as it propagates from dendrite to soma (Rall & Agon-Snir, 1998). Spines and protrusions have been previously reported on inspiratory preBötC neurons (Koizumi *et al.* 2008), but our data suggest that these spiny neurons may not be *Dbx1* derived.

Some *Dbx1*$^-$ neurons within the preBötC are *Lmx1b*-derived catecholaminergic neurons (of the C1 group), which are involved in modulating blood pressure and cardiovascular function, but are unlikely to be implicated in respiratory rhythm generation (Gray *et al.* 2010). The fraction of *Dbx1*$^-$ neurons in the present study that belongs to the C1 group is probably small, because the bulk of the C1 group lies ventral to the preBötC (Schreihofer & Guyenet, 1997).

Approximately half of the inspiratory neurons in the preBötC are reported to be inhibitory glycinergic neurons (Winter *et al.* 2009). It is therefore conceivable that *Dbx1*$^-$ neurons may be glycinergic neurons, presumably derived from transcription factor *Lbx1*, which is necessary for the development of glycinergic neurons in the ventral medulla (Pagliardini *et al.* 2008).

We also acknowledge the possibility of incomplete Cre recombination and that some of the recorded *Dbx1*$^-$ neurons were actually *Dbx1*-derived neurons that failed to express the reporter protein. We induce Cre recombination by administering tamoxifen at E10.5 to obtain robust reporter expression in hindbrain *Dbx1*$^+$ neurons (Hirata *et al.* 2009; Gray *et al.* 2010). The appearance of a vaginal plug during breeding was sometimes in doubt, and thus it is possible that tamoxifen was administered as late as E12.5 in some cases. However, *Dbx1* is expressed at E9.5 in the mouse brain and spinal cord (Lu *et al.* 1992; Shoji *et al.* 1996), and is observed even as early as E8.5 in small subsets of forebrain neurons (Causeret *et al.* 2011). Therefore, *Dbx1*$^+$ cells that appear earlier than the tamoxifen administration date would remain undetectable via fluorescent protein expression, and could constitute a subset of *Dbx1*$^-$ neurons that exhibited rhythmic properties commensurate with *Dbx1*$^+$ neurons. We contend that it is unlikely that our *Dbx1*$^-$ subpopulation is dominated by false-negative *Dbx1*$^+$ neurons, given measurable differences in morphology. It is possible that the *Dbx1*$^-$ population in the present study reflects the GABAergic or glycinergic subpopulation in the preBötC (Kuwana *et al.* 2006; Winter *et al.* 2009; Morgado-Valle *et al.* 2010).

In summary, we evaluated the membrane properties of genetically identified, putatively rhythmogenic neurons in the preBötC to help unravel the cellular mechanisms of respiratory rhythmogenesis. The rhythmogenic nature of *Dbx1*$^+$ neurons may be attributable, at least in part, to a higher level of intrinsic excitability in the context of network synaptic activity. Although it remains to be demonstrated, we propose that dendritic properties may facilitate temporal summation and integration of local synaptic inputs from other *Dbx1*$^+$ neurons, which could be important for initiating and maintaining bursts and synchronizing activity during the inspiratory phase.

References

Acker CD & White JA (2007). Roles of I_A and morphology in action potential propagation in CA1 pyramidal cell dendrites. *J Comput Neurosci* **23**, 201–216.

Bianchi AL, Denavit-Saubie M & Champagnat J (1995). Central control of breathing in mammals: neuronal circuitry, membrane properties, and neurotransmitters. *Physiol Rev* **75**, 1–45.

Biel M, Wahl-Schott C, Michalakis S & Zong X (2009). Hyperpolarization-activated cation channels: from genes to function. *Physiol Rev* **89**, 847–885.

Bouvier J, Thoby-Brisson M, Renier N, Dubreuil V, Ericson J, Champagnat J, Pierani A, Chedotal A & Fortin G (2010). Hindbrain interneurons and axon guidance signaling critical for breathing. *Nat Neurosci* **13**, 1066–1074.

Causeret F, Ensini M, Teissier A, Kessaris N, Richardson WD, Lucas de Couville T & Pierani A (2011). *Dbx1*-expressing cells are necessary for the survival of the mammalian anterior neural and craniofacial structures. *PLoS One* **6**, e19367.

Crowder EA, Saha MS, Pace RW, Zhang H, Prestwich GD & Del Negro CA (2007). Phosphatidylinositol 4,5-bisphosphate regulates inspiratory burst activity in the neonatal mouse preBötzinger complex. *J Physiol* **582**, 1047–1058.

Danneman PJ & Mandrell TD (1997). Evaluation of five agents/methods for anesthesia of neonatal rats. *Lab Anim Sci* **47**, 386–395.

Del Negro CA, Johnson SM, Butera RJ & Smith JC (2001). Models of respiratory rhythm generation in the pre-Bötzinger complex. III. Experimental tests of model predictions. *J Neurophysiol* **86**, 59–74.

Del Negro CA, Kam K, Hayes JA & Feldman JL (2009). Asymmetric control of inspiratory and expiratory phases by excitability in the respiratory network of neonatal mice *in vitro*. *J Physiol* **587**, 1217–1231.

Del Negro CA, Koshiya N, Butera RJ Jr & Smith JC (2002*a*). Persistent sodium current, membrane properties and bursting behavior of pre-Bötzinger complex inspiratory neurons in vitro. *J Neurophysiol* **88**, 2242–2250.

Del Negro CA, Morgado-Valle C & Feldman JL (2002*b*). Respiratory rhythm: an emergent network property? *Neuron* **34**, 821–830.

Del Negro CA, Morgado-Valle C, Hayes JA, Mackay DD, Pace RW, Crowder EA & Feldman JL (2005). Sodium and calcium current-mediated pacemaker neurons and respiratory rhythm generation. *J Neurosci* **25**, 446–453.

Drummond GB (2009). Reporting ethical matters in *The Journal of Physiology*: standards and advice. *J Physiol* **587**, 713–719.

Elsen FP & Ramirez JM (2005). Postnatal development differentially affects voltage-activated calcium currents in respiratory rhythmic versus nonrhythmic neurons of the pre-Bötzinger complex. *J Neurophysiol* **94**, 1423–1431.

Ezure K (1990). Synaptic connections between medullary respiratory neurons and considerations on the genesis of respiratory rhythm. *Prog Neurobiol* **35**, 429–450.

Feldman JL & Del Negro CA (2006). Looking for inspiration: new perspectives on respiratory rhythm. *Nat Rev Neurosci* **7**, 232–242.

Feldman JL, Del Negro CA & Gray PA (2013). Understanding the rhythm of breathing: so near, yet so far. *Annu Rev Physiol* **75**, 423–452.

Fox J, Barthold S, Davisson M, Newcomer C, Quimby F & Smith A, ed. (2007). *The Mouse in Biomedical Research*, 2nd edition, volume 3, *Normative Biology, Husbandry, and Models*. Academic Press, Burlington, MA, USA.

Gray PA, Hayes JA, Ling G, Llona I, Tupai S, Picardo MC, Ross S, Hirata T, Corbin JG, Eugenin J & Del Negro CA (2010). Developmental origin of preBötzinger complex respiratory neurons. *J Neurosci* **30**, 14883–14895.

Gray PA, Janczewski WA, Mellen N, McCrimmon DR & Feldman JL (2001). Normal breathing requires preBötzinger complex neurokinin-1 receptor-expressing neurons. *Nat Neurosci* **4**, 927–930.

Gray PA, Rekling JC, Bocchiaro CM & Feldman JL (1999). Modulation of respiratory frequency by peptidergic input to rhythmogenic neurons in the preBötzinger complex. *Science* **286**, 1566–1568.

Hama H, Kurokawa H, Kawano H, Ando R, Shimogori T, Noda H, Fukami K, Sakaue-Sawano A & Miyawaki A (2011). Scale: a chemical approach for fluorescence imaging and reconstruction of transparent mouse brain. *Nat Neurosci* **14**, 1481–1488.

Hayes JA & Del Negro CA (2007). Neurokinin receptor-expressing pre-Bötzinger complex neurons in neonatal mice studied in vitro. *J Neurophysiol* **97**, 4215–4224.

Hayes JA, Mendenhall JL, Brush BR & Del Negro CA (2008). 4-Aminopyridine-sensitive outward currents in preBötzinger complex neurons influence respiratory rhythm generation in neonatal mice. *J Physiol* **586**, 1921–1936.

Hirata T, Li P, Lanuza GM, Cocas LA, Huntsman MM & Corbin JG (2009). Identification of distinct telencephalic progenitor pools for neuronal diversity in the amygdala. *Nat Neurosci* **12**, 141–149.

Hoffman DA, Magee JC, Colbert CM & Johnston D (1997). K^+ channel regulation of signal propagation in dendrites of hippocampal pyramidal neurons. *Nature* **387**, 869–875.

Koizumi H & Smith JC (2008). Persistent Na^+ and K^+-dominated leak currents contribute to respiratory rhythm generation in the pre-Bötzinger complex *in vitro*. *J Neurosci* **28**, 1773–1785.

Koizumi H, Wilson CG, Wong S, Yamanishi T, Koshiya N & Smith JC (2008). Functional imaging, spatial reconstruction, and biophysical analysis of a respiratory motor circuit isolated *in vitro*. *J Neurosci* **28**, 2353–2365.

Koshiya N & Smith JC (1999). Neuronal pacemaker for breathing visualized *in vitro*. *Nature* **400**, 360–363.

Krey RA, Goodreau AM, Arnold TB & Del Negro CA (2010). Outward currents contributing to inspiratory burst termination in prebotzinger complex neurons of neonatal mice studied *in vitro*. *Front Neural Circuits* **4**, 124.

Kuwana S, Tsunekawa N, Yanagawa Y, Okada Y, Kuribayashi J & Obata K (2006). Electrophysiological and morphological characteristics of GABAergic respiratory neurons in the mouse pre-Bötzinger complex. *Eur J Neurosci* **23**, 667–674.

Lu S, Bogarad LD, Murtha MT & Ruddle FH (1992). Expression pattern of a murine homeobox gene, *Dbx*, displays extreme spatial restriction in embryonic forebrain and spinal cord. *Proc Natl Acad Sci U S A* **89**, 8053–8057.

Madisen L, Zwingman TA, Sunkin SM, Oh SW, Zariwala HA, Gu H, Ng LL, Palmiter RD, Hawrylycz MJ, Jones AR, Lein ES & Zeng H (2010). A robust and high-throughput Cre reporting and characterization system for the whole mouse brain. *Nat Neurosci* **13**, 133–140.

Magee JC (1999). Dendritic I_h normalizes temporal summation in hippocampal CA1 neurons. *Nat Neurosci* **2**, 508–514.

Migliore M, Messineo L & Ferrante M (2004). Dendritic I_h selectively blocks temporal summation of unsynchronized distal inputs in CA1 pyramidal neurons. *J Comput Neurosci* **16**, 5–13.

Morgado-Valle C, Baca SM & Feldman JL (2010). Glycinergic pacemaker neurons in preBötzinger complex of neonatal mouse. *J Neurosci* **30**, 3634–3639.

Myatt DR, Hadlington T, Ascoli GA & Nasuto SJ (2012). Neuromantic – from semi-manual to semi-automatic reconstruction of neuron morphology. *Front Neuroinform* **6**, 4.

Onimaru H, Ballanyi K & Homma I (2003). Contribution of Ca^{2+}-dependent conductances to membrane potential fluctuations of medullary respiratory neurons of newborn rats *in vitro*. *J Physiol* **552**, 727–741.

Pace RW, Mackay DD, Feldman JL & Del Negro CA (2007*a*). Role of persistent sodium current in mouse preBotzinger Complex neurons and respiratory rhythm generation. *J Physiol* **580**, 485–496.

Pace RW, Mackay DD, Feldman JL & Del Negro CA (2007*b*). Inspiratory bursts in the preBötzinger complex depend on a calcium-activated non-specific cationic current linked to glutamate receptors. *J Physiol* **582**, 113–125.

Pagliardini S, Adachi T, Ren J, Funk GD & Greer JJ (2005). Fluorescent tagging of rhythmically active respiratory neurons within the pre-Bötzinger complex of rat medullary slice preparations. *J Neurosci* **25**, 2591–2596.

Pagliardini S, Ren J, Gray PA, Vandunk C, Gross M, Goulding M & Greer JJ (2008). Central respiratory rhythmogenesis is abnormal in *Lbx1*-deficient mice. *J Neurosci* **28**, 11030–11041.

Pena F, Parkis MA, Tryba AK & Ramirez JM (2004). Differential contribution of pacemaker properties to the generation of respiratory rhythms during normoxia and hypoxia. *Neuron* **43**, 105–117.

Pierani A, Moran-Rivard L, Sunshine MJ, Littman DR, Goulding M & Jessell TM (2001). Control of interneuron fate in the developing spinal cord by the progenitor homeodomain protein Dbx1. *Neuron* **29**, 367–384.

Ptak K, Zummo GG, Alheid GF, Tkatch T, Surmeier DJ & McCrimmon DR (2005). Sodium currents in medullary neurons isolated from the pre-Bötzinger complex region. *J Neurosci* **25**, 5159–5170.

Rall W & Agon-Snir H (1998). Cable theory for dendritic neurons. In *Methods in Neuronal Modeling: from Ions to Networks*, 2nd edition, ed. Koch C & Segev I, pp. 27–92. MIT Press, Cambridge, MA, USA.

Ramirez JM, Koch H, Garcia AJ 3rd, Doi A & Zanella S (2011). The role of spiking and bursting pacemakers in the neuronal control of breathing. *J Biol Phys* **37**, 241–261.

Ramirez JM & Viemari JC (2005). Determinants of inspiratory activity. *Respir Physiol Neurobiol* **147**, 145–157.

Rekling JC, Champagnat J & Denavit-Saubié M (1996*a*). Electroresponsive properties and membrane potential trajectories of three types of inspiratory neurons in the newborn mouse brain stem in vitro. *J Neurophysiol* **75**, 795–810.

Rekling JC, Champagnat J & Denavit-Saubié M (1996*b*). Thyrotropin-releasing hormone (TRH) depolarizes a subset of inspiratory neurons in the newborn mouse brain stem in vitro. *J Neurophysiol* **75**, 811–819.

Richter DW (1982). Generation and maintenance of the respiratory rhythm. *J Exp Biol* **100**, 93–107.

Richter DW & Spyer KM (2001). Studying rhythmogenesis of breathing: comparison of *in vivo* and *in vitro* models. *Trends Neurosci* **24**, 464–472.

Ruangkittisakul A, Panaitescu B & Ballanyi K (2011). K_+ and Ca^{2+} dependence of inspiratory-related rhythm in novel "calibrated" mouse brainstem slices. *Respir Physiol Neurobiol* **175**, 37–48.

Rubin JE, Hayes JA, Mendenhall JL & Del Negro CA (2009). Calcium-activated nonspecific cation current and synaptic depression promote network-dependent burst oscillations. *Proc Natl Acad Sci U S A* **106**, 2939–2944.

Schreihofer AM & Guyenet PG (1997). Identification of C1 presympathetic neurons in rat rostral ventrolateral medulla by juxtacellular labeling in vivo. *J Comp Neurol* **387**, 524–536.

Schwarzacher SW, Smith JC & Richter DW (1995). Pre-Bötzinger complex in the cat. *J Neurophysiol* **73**, 1452–1461.

Scorcioni R, Polavaram S & Ascoli GA (2008). L-Measure: a web-accessible tool for the analysis, comparison and search of digital reconstructions of neuronal morphologies. *Nat Protoc* **3**, 866–876.

Shoji H, Ito T, Wakamatsu Y, Hayasaka N, Ohsaki K, Oyanagi M, Kominami R, Kondoh H & Takahashi N (1996). Regionalized expression of the Dbx family homeobox genes in the embryonic CNS of the mouse. *Mech Dev* **56**, 25–39.

Smith JC, Ellenberger HH, Ballanyi K, Richter DW & Feldman JL (1991). Pre-Bötzinger complex: a brainstem region that may generate respiratory rhythm in mammals. *Science* **254**, 726–729.

Tan W, Janczewski WA, Yang P, Shao XM, Callaway EM & Feldman JL (2008). Silencing preBötzinger Complex somatostatin-expressing neurons induces persistent apnea in awake rat. *Nat Neurosci* **11**, 538–540.

Thoby-Brisson M & Ramirez JM (2001). Identification of two types of inspiratory pacemaker neurons in the isolated respiratory neural network of mice. *J Neurophysiol* **86**, 104–112.

Thoby-Brisson M, Telgkamp P & Ramirez JM (2000). The role of the hyperpolarization-activated current in modulating rhythmic activity in the isolated respiratory network of mice. *J Neurosci* **20**, 2994–3005.

Volgin DV, Rukhadze I & Kubin L (2008). Hypoglossal premotor neurons of the intermediate medullary reticular region express cholinergic markers. *J Appl Physiol* **105**, 1576–1584.

Wallen-Mackenzie A, Gezelius H, Thoby-Brisson M, Nygård A, Enjin A, Fujiyama F, Fortin G & Kullander K (2006). Vesicular glutamate transporter 2 is required for central respiratory rhythm generation but not for locomotor central pattern generation. *J Neurosci* **26**, 12294–12307.

Winter SM, Fresemann J, Schnell C, Oku Y, Hirrlinger J & Hulsmann S (2009). Glycinergic interneurons are functionally integrated into the inspiratory network of mouse medullary slices. *Pflugers Arch* **458**, 459–469.

Zavala-Tecuapetla C, Aguileta MA, Lopez-Guerrero JJ, González-Marín MC & Peña F (2008). Calcium-activated potassium currents differentially modulate respiratory rhythm generation. *Eur J Neurosci* **27**, 2871–2884.

Author contributions

C.A.D.N. and M.C.D.P. conceptualized and designed the experiments. M.C.D.P. collected and analysed the electrophysiological data. K.T.H.W. and V.T.A. performed reconstructions of the morphology. C.A.D.N. and M.C.D.P. interpreted the data, wrote and revised the article. All authors approved the final version of the manuscript.

Acknowledgements

This work was supported by the National Heart, Lung, and Blood Institute (NHLBI) grant R01-HL104127-01 (principal investigator: C. A. Del Negro) and National Institute of Neurological Disorders and Stroke (NINDS) grant 1-F31-NS071860-01 (M. C. D. Picardo).